RESEARCH ARTICLE | NOVEMBER 13 2024

# Characterization of low sodium type II silicon clathrate film spin dynamics

Joseph P. Briggs ; Yinan Liu ; P. Craig Taylor ; Meenakshi Singh ; Reuben T. Collins ; Carolyn A. Koh



*Appl. Phys. Lett.* 125, 202402 (2024)
https://doi.org/10.1063/5.0230407
CHORUS

Applied Physics Letters ARTICLE pubs.aip.org/aip/apl

# Characterization of low sodium type II silicon clathrate film spin dynamics

Cite as: Appl. Phys. Lett. **125**, 202402 (2024); doi: 10.1063/5.0230407
Submitted: 23 July 2024 · Accepted: 31 October 2024 ·
Published Online: 13 November 2024

View Online Export Citation CrossMark

Joseph P. Briggs,[1] Yinan Liu,[1] P. Craig Taylor,[2] Meenakshi Singh,[2] Reuben T. Collins,[2] and Carolyn A. Koh[1,a)]

## AFFILIATIONS

[1]Department of Chemical and Biological Engineering, Colorado School of Mines, Golden, Colorado 80401, USA
[2]Department of Physics, Colorado School of Mines, Golden, Colorado 80401, USA

[a)]Author to whom correspondence should be addressed: ckoh@mines.edu

## ABSTRACT

Type II Si clathrate is a Si-based, crystalline alternative to diamond silicon with interesting optoelectronic properties. Here, a pulsed electron paramagnetic resonance study of the spin dynamics of sodium-doped, type II $Na_xSi_{136}$ silicon clathrate films is reported. Focusing on the hyperfine lines of isolated Na atoms, the temperature dependence of the electron spin dynamics is examined from 6 to 25 K. The measurements exhibit multi-exponential decay, indicating multiple spin relaxation rates in the system. As expected, spin relaxation time ($T_1$) increases rapidly with decreasing temperature, reaching ~300 $\mu$s at 6.4 K. The phase memory ($T_M$) shows less temperature dependence with a value of ~3 $\mu$s at the same temperature. The temperature dependence of $T_1$ exhibits Arrhenius behavior in the measurement range consistent with an Orbach pathway. There are strong similarities to the spin behavior of other defect donors in diamond silicon. The results provide insights into the potential of Si clathrates for spin-based applications.





Silicon clathrates are open, cage-like, crystalline allotropes of Si. These metastable semiconducting alternatives to common diamond cubic Si (d-Si) are predicted to have potentially important optoelectronic properties.[1–6] Synthesis of Si clathrates, however, typically results in the inclusion of interstitial guest atoms inside the cages.[7–12] The guests, generally alkali or alkaline earth metals, contribute electrons to the host lattice leading to metallic behavior. For type I Si clathrate, the cages tend to be completely filled, and the material is essentially metallic.[7,8] In contrast, for type II Si clathrate the guest concentration can vary ($M_xSi_{136}$, where $0 < x < 24$.)[10] If the guest concentration can be sufficiently reduced, semiconducting properties are recovered and the guest becomes an n-type dopant.[13–15]

The most common route to synthesis of type II Si clathrate involves decomposition of a NaSi precursor.[10,16–18] As a result, the properties of Na guests have been studied extensively. Using combinations of processes including thermal diffusion, treatment with iodine, and post synthesis etching, Na concentrations as low as $10^{18}$ cm$^{-3}$ have been reported.[4,11,19,20] This is a regime where the clathrate can be viewed as a heavily doped semiconductor. Band structure calculations suggest that type II Si clathrate should be direct or quasi-direct, with a bandgap near 2.0 eV.[2,21–23] Experimental studies of low Na content clathrate have reported tunable bandgaps near 1.7 eV, absorption coefficients hundreds of times larger than d-Si, and photoluminescence (PL) emission near room temperature.[6,19] This has led to considerable interest in the possible photovoltaic and optoelectronic applications of the material.

The properties of the Na donor inside the clathrate cages are also of considerable interest. For example, the type II structure is composed of small $Si_{20}$ and large $Si_{28}$ cages with the small cages emptying first leaving only some large cages occupied at low Na concentrations.[24] Using continuous wave electron paramagnetic resonance (CW-EPR) spectra, the strength of hyperfine interactions between the donated electron, the Na nucleus, and naturally occurring $^{29}$Si isotopes on the cage have been used to infer that about 42% of the donor wavefunction lies within the cage, and only about 20% extends beyond the surrounding cage.[15,25] At the same time, the temperature dependence of the Na hyperfine lines and of PL emission suggest a shallow donor with a binding energy of only 10–20 meV.[3,19]

There are some key parameters that are often used to determine a material's potential for storing information as a qubit. These include the longitudinal relaxation time also known as the spin–lattice relaxation time ($T_1$) and the phase memory ($T_M$), which encompasses coherence time ($T_2$) or spin–spin relaxation, spectral, spin, and instantaneous diffusion. Nitrogen-vacancy centers in diamond and

phosphorus in d-Si (Si:P) have been at the forefront of the research for defect-based quantum materials.[26–34] However, due to limitations of these systems other directions are being explored. For Si, this includes other group V donors,[35,36] group VI impurities,[37] acceptors,[38] and defect complexes in related compounds like silicon carbide.[39–41] Since similarities between guests in Si clathrates to donors in d-Si have been drawn, it is interesting to ask if the donor electron of guests in Si clathrates could have equivalent properties or alleviate limitations of other Si defects for quantum applications.[4,15] The cage-like structure of fullerenes, which could be seen as an analog to Si clathrates has also gained attention for application in quantum computing.[42,43] While spin relaxation dynamics have been explored in many of these systems, no such work has been done in type II Si clathrates.[35,44–48]

In this work we present a temperature dependent investigation of the field swept echo spectrum, $T_1$, and $T_M$ times of the Na donor in type II Si clathrate. We also compare the results to other more heavily studied Si-based defect states and discuss the possible advantages and disadvantages of the type II Si clathrate material and the potential for increasing spin coherence times in this system.

The type II $Na_xSi_{136}$ ($x \sim 0.009$) Si clathrate film samples were prepared by adapting a procedure from Ref. 10 and detailed further in the supplementary material. As a first step in exploring the spin dynamics of donors in silicon clathrates, it was necessary to determine if an echo could be detected. It is important to note the Na concentrations of these samples, while low for clathrates, are still higher than doping levels where spin echoes of donors in d-Si have been observed.[44] Field swept echo pulsed spectra were acquired using a Hahn echo detection sequence ($\pi/2$–$\tau$–$\pi$–$\tau$–echo) while sweeping a magnetic field at 9.81 GHz. 16 ns $\pi/2$ and 32 ns $\pi$ pulses were used with the delay between pulses, $\tau$, fixed at 400 ns. These values were selected to fully excite the echo while minimizing the effects of resonator ringdown. They are also common pulse durations, simplifying comparisons to other systems.[45,46,49,50] A CW-EPR spectrum of the sample was acquired at 9.45 GHz and integrated to obtain the adsorption curve. The comparison between the CW and pulsed-EPR spectra is shown in Fig. 1. The CW-EPR spectra were shifted in field to account for the different measurement frequencies, which allows for a direct comparison to the pulsed-EPR spectrum.

The spectra exhibit several key features that have previously been discussed in CW-EPR studies of type II Si clathrate.[3,4,15,51] Of particular interest here are four hyperfine lines at 325, 337, 352, and 365 mT associated with interactions of the electron and the four spin 3/2 nuclear states of an isolated Na guest. Other notable features include weak superhyperfine lines surrounding and between each of the hyperfine lines, which have been attributed to Na pairs in neighboring cages and interactions between the Na donor electron and spin active $^{29}Si$ residing on the clathrate cage.[3,4,15,51] Additionally, there is a broad feature centered around 344 mT attributed to a signal from Na clusters with varying amounts of Na in neighboring cages.[15] While this signal is quite strong in the integrated CW-EPR spectrum, it is indistinguishable from background in the pulsed spectrum. There is also a prominent feature consistent with dangling bonds in disordered or amorphous silicon (a-Si) at around 349 mT, seen as the tallest peak in the integrated CW-EPR spectrum and as a shoulder in the field swept echo spectrum.[15,51]

The CW-EPR spectrum of other donors in d-Si shows many of the same features, including hyperfine lines associated with the nuclear

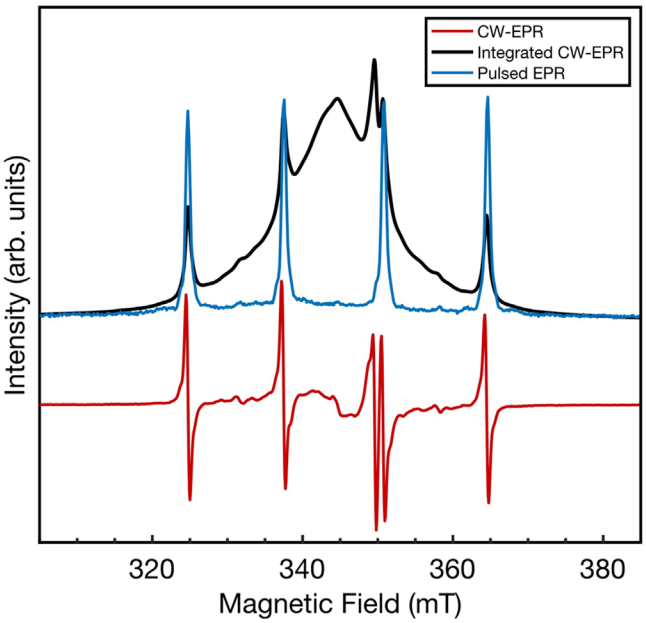


**FIG. 1.** $Na_xSi_{136}$ type II clathrate film EPR spectra. Pulsed-EPR field swept echo (blue) compared to CW-EPR (red) and integrated absorption (black) all taken at 6.4 K. The field swept echo spectrum was averaged over three scans and the CW-EPR spectrum was averaged over ten scans.

spin of the defect, fine structure attributed to defect pairs, and a broad peak associated with clusters.[4,15,46,52] A reduction in the size of the broad feature relative to the hyperfine lines is also observed in field swept echo experiments of Si:P where the authors stated part of this feature likely arises from a homogeneous excitation, which cannot be detected in a spin echo signal.[44] In the present case, since the broad background is formed from interacting Na clusters, we suspect the echoes are decaying too fast to be observed in the field swept echo spectrum. Varying $\tau$ from 200 ns to 1.8 $\mu$s, with 200 ns being the lowest $\tau$ possible without experiencing significant ringdown from the pulse sequence, did not result in an increase in this signal. This supports that decay time is responsible for this observation and the echo from the spins making up the broad feature decays faster than 200 ns. This faster decay is expected due to Na spin–spin interactions in the clustered phase. The lower relative strength of the dangling bond signal in the pulsed spectrum is attributed to saturation effects arising from the longer relaxation times of the dangling bond signal relative to the hyperfine lines. This is apparent in the series of spectra in Fig. S3. By analyzing the distinct temporal dependencies of the contributions to the EPR signal, it is possible to separate and isolate the Na hyperfine interactions. This allows for the measurement of $T_1$, the interaction of the Na donor electron transferring energy to the Si lattice, and $T_M$, the length of time the donor electron spins can stay in phase. These relaxation times are essential for understanding the spin dynamics and relationships within the system.

To measure $T_1$, a standard inversion recovery sequence ($\pi$–$t$–$\pi/2$–$\tau$–$\pi$–$\tau$–echo) was used with 16 ns $\pi/2$ and 32 ns $\pi$ pulses for the detection sequence. The inversion (first $\pi$) pulse was then optimized to produce the strongest signal and was between 28 and 34 ns. The time $t$

between the inversion pulse and detection sequence was increased stepwise while $\tau$ was kept constant at 400 ns. The net magnetization was recorded as a function of $t$. Each inversion recovery experiment was performed with the field centered around the highest field hyperfine line around 365 mT at 9.81 GHz to avoid overlap with the dangling bond and broad clustered Na related features, which have different decay rates as mentioned above.

Figure 2 shows inversion recovery results for the low Na concentration sample. Measurements were taken from 6.4 K (the lowest temperature achieved by the equipment) up to 25 K, the highest temperature where an echo could be detected. However, above ~15 K, the magnitude of the inverted echo, even with high averaging, became difficult to detect above the noise, and fits to obtain $T_1$ were unreliable. The inset to Fig. 2 shows inversion recovery measurements for two temperatures on a linear scale offset for clarity. As time increases, the echo intensity levels off at a value of net magnetization corresponding to when the electrons have returned to their ground state. It is clear from Fig. 2 that as temperature decreases $T_1$ increases as expected. Inverting the measurements and subtracting this baseline value allows the inversion recovery data to be plotted on the semilog plot shown in the main part of Fig. 2. If the change in intensity resulted from a single decay component, an exponential could be used to obtain $T_1$. This is not the case with the measurements being clearly nonlinear in the semilog plot. A biexponential of the form of the equation below was determined to describe $T_1$ more accurately as the simplest explanation that fit the data,

$$M_Z(t) = M_{0s}\left[1 - 2e^{\frac{-t}{T_{1s}}}\right] + M_{0f}\left[1 - 2e^{\frac{-t}{T_{1f}}}\right]. \quad (1)$$

In this expression, $M_Z$ is the net spin magnetization, $M_0$ being the total spin magnetization, $T_1$ the relaxation time, with $f$ and $s$ denoting fast and slow relaxation components, respectively. Two such fits are shown by the black dashed lines in the main part of Fig. 2 and in the inset. Non-exponential inversion recovery curves are observed in many systems and have been attributed to inhomogeneity, anisotropy, and native defects in combination with spectral diffusion.[53–55] The slower decaying term in the biexponential is expected to be more representative of an isolated Na guest and places a lower bound on the intrinsic value of $T_1$.[56]

A close inspection of the fits shows that this biexponential form still does not completely describe the decay, which could be an indication of multiple relaxation times at work. Rather than attempt a multi-exponential fit, the initial slope and the tail end linear region of the measurements on the semilog plot were independently fit to exponentials as shown in Fig. S5(a). Saturation recovery experiments, which are an alternative method for obtaining $T_1$, gave essentially the same $T_1$ values increasing confidence in the results, shown in Fig. S5(b).

The temperature dependence of both components is shown in an Arrhenius plot in Fig. 3. The fast and slow relaxation rates exhibit thermally activated behavior in the temperature range of the measurement with similar activation energies. The slope of the slow rate gives an activation energy of $\Delta E = 41$ K corresponding to 3.5 meV. For similar donor defects in d-Si, thermally activated behavior is observed in the same temperature range and is attributed to a two-phonon Orbach mechanism.[45,54,57–59]

The reported activation energies, ranging from around 125 K for P[45] to 500 K in Bi,[49] are associated with the ground state to first excited state excitation energy of the donor, which is determined by valley orbit splitting.[36,45,49] The activated behavior observed here is consistent with an Orbach process, but with a smaller activation energy. This is

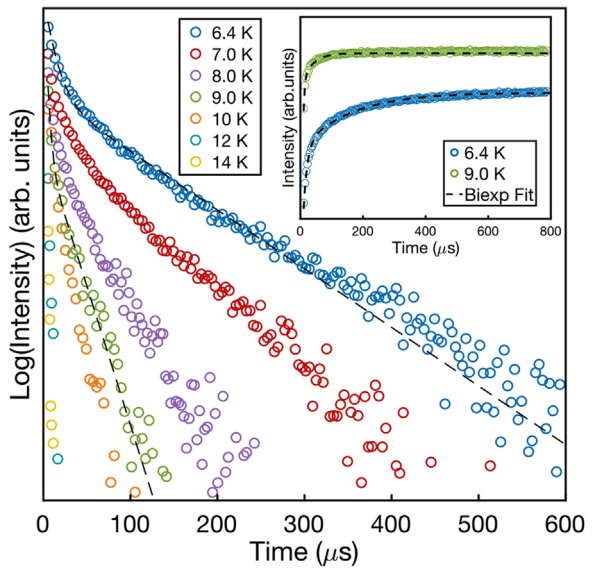


**FIG. 2.** Semilog plot of the inversion recovery measurements of $Na_xSi_{136}$ type II Si clathrate. The black dashed lines represent the biexponential $T_1$ fit. The inset shows the linear plot of the measurements at 6.4 and 9 K. The field was centered at the Na hyperfine line around 365 mT at 9.81 GHz to measure the echo intensity for all measurements.

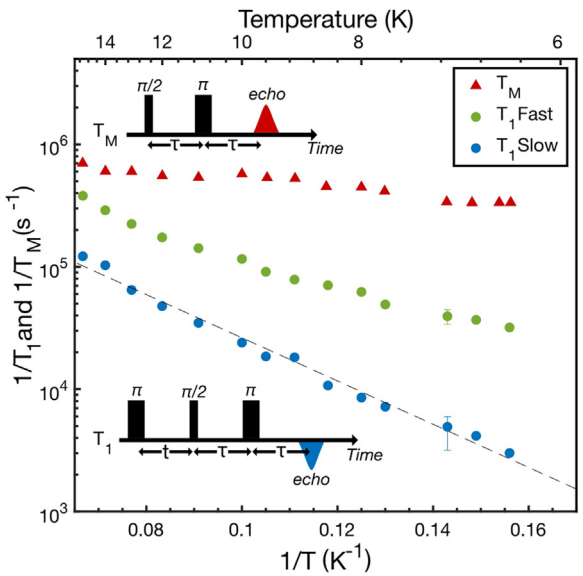


**FIG. 3.** Arrhenius plot of the $T_1$ times and $T_M$ times for low sodium $Na_xSi_{136}$ type II Si clathrate film. The measurements were centered at 365 mT and 9.81 GHz. The $T_1$ times are broken into the slow decaying relaxation time in blue and fast-decaying component in green with the inversion recovery pulse sequence shown at the bottom left. $T_M$ times are shown in red with the echo decay pulse sequence at the top left.

potentially in line with the smaller reported donor binding energy of Na in type II silicon clathrate (10–20 meV) relative to d-Si donors.[3,15,36,60,61] However, much less is known about the band structure of type II Si clathrate, which has been reported to have a direct or quasi-direct bandgap, which could lead to additional conduction band degeneracies. We note that the temperature dependence of $T_1$ did not fit other processes such as the Raman mechanism, which would likely require lower temperatures to test if it were active. The error bars in the curve were calculated at 7 K and discussed further in Fig. S5(a).

To measure $T_M$, an echo decay sequence ($\pi/2$–$\tau$–$\pi$–$\tau$–echo) was used with 16 ns $\pi/2$ and 32 ns $\pi$ pulses. The amplitude of the echo ($I$) was measured while $\tau$ was incremented. The echo decay measurements are shown in Fig. S6. The decays deviated less from an exponential than the inversion recovery results discussed above. The $T_M$ values reported in Fig. 3 were taken from single exponential fits of the form $I(2\tau) = I_0 e^{-(2\tau/T_M)}$ at all temperatures. Error bars were calculated at 6.4 K and were less than the marker size in the figure.

$T_M$ is quite a bit faster and exhibits much less temperature dependence than $T_1$. $T_M$ in many systems including d-Si is strongly affected by dipole–dipole and spin–spin related spectral diffusion processes knocking spins out of phase with each other.[27,62,63] Similarly it seems likely that spectral diffusion is dominating the $T_M$ times obtained here. In studies of isotopically purified d-$^{28}$Si doped with P and Bi, $T_M$ was comparable to and bounded by $T_1$ following the same temperature dependence until near 10–14 K.[49,64] Below this temperature $T_M$ saturated. In P doped d-$^{28}$Si the concentration dependence was studied with saturation temperature higher and $T_M$ shorter, when doping was increased from $10^{15}$ to $10^{16}$ cm$^{-3}$.[64] Naturally occurring Si:P shows a similar concentration dependence in $T_M$.[44,65] The Na doping of the clathrate samples studied here is much higher at $\sim 10^{18}$ cm$^{-3}$. The lack of temperature dependence we observe could indicate saturation of $T_M$ in the temperature range of this study. As an initial attempt to test this, a comparison was made between a lower and more highly Na doped clathrate sample (dopant density $\sim 10^{18}$ and $\sim 10^{20}$ cm$^{-3}$, respectively). The low Na sample only exhibited a very slight increase in $T_M$.

The spin dynamics of defects in non-diamond silicon allotropes are an exciting previously under explored property in these material systems. Since this is the first reported study of pulsed-EPR of a guest donor atom in a Si clathrate, it is interesting to make comparisons to $T_1$ and $T_M$ studies of other donors in Si, which are being heavily investigated as potential quantum materials.[36,45,49,66,67] The $T_1$ and $T_M$ times reported here are clearly much smaller than have been reported for highly optimized, high purity, isotopically purified d-Si with low donor doping.[49,64] At the same time, decay times drop rapidly with doping in d-Si and there are no reports of relaxation time measurements for donor concentrations in the higher range studied here. We speculate the nature of the Na donor wavefunction may mitigate some of the effects of high doping. The s-like ground state wavefunction of a donor in d-Si extends over many lattice sites.[48] In contrast, 80% of the probability density of the electron bound to Na in the clathrate resides in or on the Si cage surrounding the Na atom.[15] This should lead to less sensitivity to dopants in neighboring cages and may help explain why we have detected spin echoes with higher doping concentrations at levels of $10^{18}$–$10^{19}$ cm$^{-3}$. In addition, d-Si has an indirect bandgap while type II Si clathrate is much more optically efficient, as discussed above, opening up the possibility of addressing spin coupled electronic states in the Si clathrate optically in a manner not possible in d-Si.

Of particular concern, however, are the low binding energy that has been reported for Na in type II clathrate and the low activation energy of the temperature dependence of $T_1$ in the present study.[3] At 15 K, $T_1$ for donors in naturally occurring Si and for Na in type II clathrate are comparable, but when the temperature is reduced to near 6 K, $T_1$ for d-Si is orders of magnitudes longer.[36,45] If these values prove to be intrinsic, it would indicate the need for extremely low temperatures to obtain a useful $T_M$. The multi-exponential decay curve is also of importance as the fast-decaying component of $T_1$ could be detrimental to spin-based applications. The same tight wavefunction that reduces sensitivity to defects on nearby cages could increase sensitivity to defects on the surrounding cage requiring further advancements in material quality.

These observations suggest several critical future research directions to enhance the understanding of spin relaxation dynamics in guest-doped type II Si clathrate and to evaluate the potential for this material for quantum applications. The first is a focus on material quality. We note that the $T_1$ and $T_M$ values reported here should be viewed as lower bounds. As the synthesis of these materials continues to be advanced and refined, decreased dopant concentrations coupled with improved film quality should lead to improved $T_1$ and $T_M$, and address the question of how close to optimized d-Si they can come and if $T_M$, values can be pushed closer to $T_1$, as discussed above. This in turn might allow the temperature where relaxation is observed to be extended, which would be helpful in applications. In addition, studies of alternative guests that might be more tightly bound could help unravel the temperature dependence.

See the supplementary material for further information on the clathrate film synthesis and characterization, additional details on the field swept echo and relaxation measurements, and the saturation recovery and echo decay measurements.

This work was supported by the National Science Foundation, Grant No. 2114569. This work was done in collaboration with the National Renewable Energy Laboratory, and the authors would like to acknowledge David Muller and Justin Johnson for training and discussion on the E-580 Pulsed-EPR system and results.

## AUTHOR DECLARATIONS

### Conflict of Interest

The authors have no conflicts to disclose.

### Author Contributions

**Joseph P. Briggs:** Data curation (equal); Formal analysis (equal); Investigation (equal); Methodology (equal); Writing – original draft (equal); Writing – review & editing (equal). **Yinan Liu:** Formal analysis (equal); Methodology (supporting); Writing – review & editing (supporting). **P. Craig Taylor:** Conceptualization (equal); Formal analysis (supporting); Methodology (supporting). **Meenakshi Singh:** Conceptualization (equal); Formal analysis (equal); Funding acquisition (equal); Project administration (supporting); Resources (equal); Writing – review & editing (supporting). **Reuben T. Collins:** Conceptualization (equal); Formal analysis (equal); Funding acquisition (equal); Methodology (equal); Resources (lead); Supervision (lead); Writing – original draft (supporting); Writing – review & editing (lead). **Carolyn A. Koh:** Conceptualization (equal); Formal

analysis (equal); Funding acquisition (equal); Project administration (equal); Supervision (equal); Writing – review & editing (equal).

## DATA AVAILABILITY

The data that support the findings of this study are available from the corresponding author upon reasonable request.

## REFERENCES


[1]L. Krishna, A. D. Martinez, L. L. Baranowski, N. P. Brawand, C. A. Koh, V. Stevanovic, M. T. Lusk, E. S. Toberer, and A. C. Tamboli, Proc. SPIE **8981**, 898108 (2014).
[2]J. Gryko, P. F. McMillan, R. F. Marzke, G. K. Ramachandran, D. Patton, S. K. Deb, and O. F. Sankey, Phys. Rev. B **62**, R7707 (2000).
[3]H. Yahiro, K. Yamaji, M. Shiotani, S. Yamanaka, and M. Ishikawa, Chem. Phys. Lett. **246**, 167 (1995).
[4]A. Ammar, C. Cros, M. Pouchard, N. Jaussaud, J. M. Bassat, G. Villeneuve, M. Duttine, M. Ménétrier, and E. Reny, Solid State Sci. **6**, 393 (2004).
[5]M. Beekman and G. S. Nolas, J. Mater. Chem. **18**, 842 (2008).
[6]T. Fix, R. Vollondat, A. Ameur, S. Roques, J. L. Rehspringer, C. Chevalier, D. Muller, and A. Slaoui, J. Phys. Chem. C **124**, 14972 (2020).
[7]J. S. Kasper, P. Hagenmuller, M. Pouchard, and C. Cros, Science **150**, 1713 (1965).
[8]C. Cros, M. Pouchard, and P. Hagenmuller, J. Solid State Chem. **2**, 570 (1970).
[9]G. S. Nolas, *Springer Series in Material Science* (Springer, 2014), Vol. 199.
[10]L. Krishna, L. L. Baranowski, A. D. Martinez, C. A. Koh, P. C. Taylor, A. C. Tamboli, and E. S. Toberer, CrystEngComm **16**, 3940 (2014).
[11]T. Kume, F. Ohashi, K. Sakai, A. Fukuyama, M. Imai, H. Udono, T. Ban, H. Habuchi, H. Suzuki, T. Ikari, S. Sasaki, and S. Nonomura, Thin Solid Films **609**, 30 (2016).
[12]A. Dopilka, J. M. Weller, A. Ovchinnikov, A. Childs, S. Bobev, X. Peng, and C. K. Chan, Adv. Energy Sustainability Res. **2**, 2000114 (2021).
[13]N. F. Mott, J. Solid State Chem. **6**, 348 (1973).
[14]S. B. Roy, K. E. Sim, and A. D. Caplin, Philos. Mag. B **65**, 1445 (1992).
[15]W. K. Schenken, Y. Liu, L. Krishna, A. A. Majid, C. A. Koh, P. C. Taylor, and R. T. Collins, Phys. Rev. B **101**, 245204 (2020).
[16]R. Vollondat, S. Roques, C. Chevalier, J. Bartringer, J. L. Rehspringer, A. Slaoui, and T. Fix, J. Alloys Compd. **903**, 163967 (2022).
[17]F. Ohashi, M. Hattori, T. Ogura, Y. Koketsu, R. Himeno, T. Kume, T. Ban, T. Iida, H. Habuchi, H. Natsuhara, and S. Nonomura, J. Non-Cryst. Solids **358**, 2134 (2012).
[18]G. K. Ramachandran, J. Dong, J. Diefenbacher, J. Gryko, R. F. Marzke, O. F. Sankey, and P. F. McMillan, J. Solid State Chem. **145**, 716 (1999).
[19]Y. Liu, W. K. Schenken, L. Krishna, A. A. A. Majid, T. E. Furtak, M. Walker, C. A. Koh, P. C. Taylor, and R. T. Collins, Appl. Phys. Rev. **8**, 041408 (2021).
[20]Y. Liu, J. P. Briggs, A. A. Majid, T. E. Furtak, M. Walker, M. Singh, C. A. Koh, P. C. Taylor, and R. T. Collins, Inorg. Chem. **62**, 6882 (2023).
[21]G. B. Adams, M. O'Keeffe, A. A. Demkov, O. F. Sankey, and Y.-M. Huang, Phys. Rev. B **49**, 8048 (1994).
[22]A. A. Demkov, O. F. Sankey, K. E. Schmidt, G. B. Adams, and M. O'Keeffe, Phys. Rev. B **50**, 17001 (1994).
[23]R. Himeno, T. Kume, F. Ohashi, T. Ban, and S. Nonomura, J. Alloys Compd. **574**, 398 (2013).
[24]J. G. Slingsby, N. A. Rorrer, L. Krishna, E. S. Toberer, C. A. Koh, and C. M. Maupin, Phys. Chem. Chem. Phys. **18**, 5121 (2016).
[25]K. E. Sim, "Experimental studies of sodium–silicon clathrate compounds," Ph. D. thesis (University of London, 1983).
[26]B. E. Kane, Nature **393**, 133 (1998).
[27]E. Abe, J. Isoya, and K. M. Itoh, Physica B **376–377**, 28 (2006).
[28]T. D. Ladd and M. S. Carroll, Encyclopedia Mod. Opt. **1–5**, 467 (2018).
[29]E. Abe and K. M. Itoh, *Defects in Advanced Electronic Materials and Novel Low Dimensional Structures* (Elsevier, 2018) pp. 241–263.
[30]J. J. Morton, D. R. McCamey, M. A. Eriksson, and S. A. Lyon, Nature **479**, 345 (2011).
[31]L. Fricke, S. J. Hile, L. Kranz, Y. Chung, Y. He, P. Pakkiam, M. G. House, J. G. Keizer, and M. Y. Simmons, Nat. Commun. **12**, 3323 (2021).
[32]M. C. Cambria, A. Norambuena, H. T. Dinani, G. Thiering, A. Gardill, I. Kemeny, Y. Li, V. Lordi, Á. Gali, J. R. Maze, and S. Kolkowitz, Phys. Rev. Lett. **130**, 256903 (2023).
[33]N. Bar-Gill, L. M. Pham, A. Jarmola, D. Budker, and R. L. Walsworth, Nat. Commun. **4**, 1743 (2013).
[34]T. D. Ladd, F. Jelezko, R. Laflamme, Y. Nakamura, C. Monroe, and J. L. O'Brien, Nature **464**, 45 (2010).
[35]G. Feher and E. A. Gere, Phys. Rev. **114**, 1245 (1959).
[36]T. G. Castner, Phys. Rev. Lett. **8**, 13 (1962).
[37]M. Steger, A. Yang, M. L. Thewalt, M. Cardona, H. Riemann, N. V. Abrosimov, M. F. Churbanov, A. V. Gusev, A. D. Bulanov, I. D. Kovalev, A. K. Kaliteevskii, O. N. Godisov, P. Becker, H. J. Pohl, E. E. Haller, and J. W. Ager, Phys. Rev. B **80**, 115204 (2009).
[38]J. Salfi, M. Tong, S. Rogge, and D. Culcer, Nanotechnology **27**, 244001 (2016).
[39]D. Simin, H. Kraus, A. Sperlich, T. Ohshima, G. V. Astakhov, and V. Dyakonov, Phys. Rev. B **95**, 161201 (2017).
[40]J. R. Weber, W. F. Koehl, J. B. Varley, A. Janotti, B. B. Buckley, C. G. Van De Walle, and D. D. Awschalom, Proc. Natl. Acad. Sci. U. S. A. **107**, 8513 (2010).
[41]W. F. Koehl, B. B. Buckley, F. J. Heremans, G. Calusine, and D. D. Awschalom, Nature **479**, 84 (2011).
[42]C. Knapp, K.-P. Dinse, B. Pietzak, M. Waiblinger, and A. Weidinger, Chem. Phys. Lett. **272**, 433 (1997).
[43]W. Harniet, *Endohedral Fullerenes: Electron Transfer and Spin* (Springer, 2017) pp. 297–324.
[44]M. Chiba and A. Hirai, J. Phys. Soc. Jpn. **33**, 730 (1972).
[45]A. M. Tyryshkin, S. A. Lyon, A. V. Astashkin, and A. M. Raitsimring, Phys. Rev. B **68**, 193207 (2003).
[46]M. Belli, M. Fanciulli, and D. Batani, Phys. Rev. B **89**, 115207 (2014).
[47]J. Isoya, M. Katagiri, T. Umeda, S. Koizumi, H. Kanda, N. T. Son, A. Henry, A. Gali, and E. Janzén, Physica B **376–377**, 358 (2006).
[48]E. Abe, A. M. Tyryshkin, S. Tojo, J. J. Morton, W. M. Witzel, A. Fujimoto, J. W. Ager, E. E. Haller, J. Isoya, S. A. Lyon, M. L. Thewalt, and K. M. Itoh, Phys. Rev. B **82**, 121201 (2010).
[49]G. W. Morley, M. Warner, A. M. Stoneham, P. T. Greenland, J. Van Tol, C. W. Kay, and G. Aeppli, Nat. Mater. **9**, 725 (2010).
[50]M. Fehr, A. Schnegg, B. Rech, K. Lips, O. Astakhov, F. Finger, C. Freysoldt, R. Bittl, and C. Teutloff, J. Non-Cryst. Solids **358**, 2067 (2012).
[51]M. Yamaga, T. Kishita, K. Goto, S. Sunaba, T. Kume, T. Ban, R. Himeno, F. Ohashi, and S. Nonomura, J. Phys. Chem. Solids **140**, 109358 (2020).
[52]D. New and T. G. Castner, Phys. Rev. B **29**, 2077 (1984).
[53]A. Komarovskikh, M. Uvarov, V. Nadolinny, and Y. Palyanov, Phys. Status Solidi A **215**, 1800193 (2018).
[54]B. C. Rose, G. Thiering, A. M. Tyryshkin, A. M. Edmonds, M. L. Markham, A. Gali, S. A. Lyon, and N. P. De Leon, Phys. Rev. B **98**, 234140 (2018).
[55]J. S. Chen, K. J. Trerayapiwat, L. Sun, M. D. Krzyaniak, M. R. Wasielewski, T. Rajh, S. Sharifzadeh, and X. Ma, Nat. Commun. **14**, 848 (2023).
[56]K. Bader, M. Winkler, and J. Van Slageren, Chem. Commun. **52**, 3623 (2016).
[57]D. A. Redman, S. Brown, R. H. Sands, and S. C. Rand, Phys. Rev. Lett. **67**, 3420 (1991).
[58]R. Orbach, Proc. Phys. Soc. **77**, 821 (1961).
[59]K. N. Shrivastava, Phys. Status Solidi B **117**, 437 (1983).
[60]H. T. Hui, Solid State Commun. **154**, 19 (2013).
[61]N. R. Butler, P. Fisher, and A. K. Ramdas, Phys. Rev. B **12**, 3200 (1975).
[62]R. E. George, W. Witzel, H. Riemann, N. V. Abrosimov, N. Nötzel, M. L. Thewalt, and J. J. Morton, Phys. Rev. Lett. **105**, 067601 (2010).
[63]D. Goldfarb and S. Stoll, *EPR Spectroscopy: Fundamentals and Methods* (John Wiley & Sons, 2018).
[64]A. M. Tyryshkin, S. Tojo, J. J. Morton, H. Riemann, N. V. Abrosimov, P. Becker, H. J. Pohl, T. Schenkel, M. L. Thewalt, K. M. Itoh, and S. A. Lyon, Nat. Mater. **11**, 143 (2012).
[65]J. P. Gordon and K. D. Bowers, Phys. Rev. Lett. **1**, 368 (1958).
[66]D. K. Park, S. Park, H. Jee, and S. Lee, Sci. Rep. **9**, 2951 (2019).
[67]E. S. Petersen, A. M. Tyryshkin, J. J. Morton, E. Abe, S. Tojo, K. M. Itoh, M. L. Thewalt, and S. A. Lyon, Phys. Rev. B **93**, 161202 (2016).